Journal of Solid State Chemistry **159,** 174–180 (2001)
doi:10.1006/jssc.2001.9147, available online at http://www.idealibrary.com on IDEAL®

Novel Rare Earth Boron-Rich Solids

Fuxiang Zhang, Andreas Leithe-Jasper,[1] Jun Xu, Takao Mori, Yoshio Matsui, and Takaho Tanaka[2]

National Institute for Research in Inorganic Materials (NIRIM), Namiki 1-1, Tsukuba, Ibaraki 305-0041, Japan

and

Shigeru Okada

Faculty of Engineering, Kokushikan University, 4-28-1 Setagaya, Tokyo 154-8515, Japan

Received December 1, 2000; in revised form February 26, 2001; accepted March 15, 2001

A new series of boron-rich solids $ReB_{22}C_2N$ (*Re*: Y, Ho, Er, Tm, Lu) were synthesized by traditional solid-state reaction. The crystal structure of the representative compound $YB_{22}C_2N$ was solved by direct method from powder X-ray diffraction (XRD) data and transmission electron microscope (TEM) analysis. The unit cell of the new structure is rhombohedral with space group *R*-3*m* (No. 166), lattice constant $a = b = 5.623(0)$ Å and $c = 44.785(3)$ Å with six formula units in one unit cell. The atoms of boron in the solids, like most of the boron-rich solids, exist with icosahedral and octahedral clusters, and the whole crystal shows a layered structure. The interconnected nine layers of icosahedron and three layers of octahedron in a unit cell build the whole framework of the new phase and rare earth metal atoms reside in voids of the octahedron layers. The neighboring icosahedral layers link through C–B–C chains besides the direct bonding of B–B. Both experimental and structural analysis indicated that the nitrogen atoms in the new phase can be replaced with carbon. © 2001 Academic Press

Key Words: **boron-rich solids; $ReB_{22}C_2N$; icosahedron; octahedron; XRD; TEM.**

1. INTRODUCTION

Boron has the widest structural varieties in its compounds from low to high boron contents, especially boron-rich solids have attracted considerable experimental and theoretical interest because of their unusual bonding and transport properties (1–6). The boron atoms in boron-rich solids usually form very stable clusters, such as an octahedron, an icosahedron, and other polyhedrons. Such structure characteristics, which are covalently bonded with each other and form a rigid three-dimensional framework, determine their bulk properties of high hardness and refractory nature. B_4C and B_6O are typical representatives in binary systems (2, 3), which show very high hardness just after diamond and cubic BN. Recently, many new ternary compounds have been synthesized in rare earth boron-rich carbon systems (7–9). In addition, many rare earth boroncarbides have been found in the low boron content region by researchers such as Bauer (10, 11) and Rogl (12). Many of these new compounds show some interesting structures and properties.

Very recently, our group found a family of new boron-rich compounds of $ReB_{17}CN$ (*Re*: Sc, Y, Ho, Er, Tm, Lu) in the quaternary system (13). During further investigation, another new series of compounds was found in the same quaternary system except in the case of Sc. The structure is solved from powder X-ray diffraction (XRD) data with direct method, and the final result is also refined using the standard Rietveld method. The obtained structure model was confirmed by high-resolution transmission electron microscope (HRTEM) observations.

2. EXPERIMENTAL

The powdery ReB_n, amorphous boron (3N, SB-Boron Inc., USA) and pure graphite (3N, Koujundo Kagaku Co., Japan) were used as the starting material. YB_4 and YB_6 are commercial products (99.9%, CERAC, USA, and Japan New Metal Co. Ltd., respectively) and other rare earth metal borides are prepared by boro thermal reduction method from the corresponding oxides respectively (7). In order to introduce nitrogen atoms into the starting material, BCN precursor prepared from urea–boric acid-saccarose at 1400°C for 2 h were used. The starting samples with various compositions were well mixed in acetone and pressed into pellets with hydrostatic pressure of 250 MPa or so before

[1] To whom correspondence should be addressed. E-mail: tanakat@nirim.go.jp.

[2] Present address: MPI—CPFS, Dresden, Bayeuther Straße-40, D-01187, Germany.

0022-4596/01 $35.00

heating. The pellets reacted in a BN or graphite crucible which was inserted into an inductively heated graphite susceptor. The reaction process was performed in vacuum of 10^{-4} Pa and maintained at a predetermined temperature of about 1700°C using a RF furnace for 8 to 12 h. In order to ensure the uniform composition, each sample was crushed, reshaped, and subjected to at least a second heating.

The phase composition of the reacted products was monitored by powder XRD. A pure single phase could be obtained in a wide metal/nonmetal composition ratio in the Y–B–C(–N) system if the B/C ratio was controlled properly. In some cases, a small amount of ReB_4, ReB_6, and ReB_{12} appeared in the final reacted products, which can be removed by diluted nitric acid ($HNO_3/H_2O = 1{:}2$) at 100°C for several minutes, this process did not cause the decomposition of the new phase. The structure determination was carried out using a standard high-resolution powder X-ray diffractometer (R-2000, Rigaku Co.) with Cu$K\alpha$ radiation. The scanning step width was 0.02° in 2θ and sampling time was 6 s. The composition of boron and yttrium in the new phase was determined by an inductively coupled plasma atomic emission spectroscopy analysis after the sample was dissolved into conc. HNO_3 + conc. HCl (1:1) solution by keeping it in an air-tight vessel at 110°C for about 12 h. The carbon content was determined by a volumetric combustion method using a carbon determinator (LECO CS-444) and nitrogen was determined with a standard inert gas fusion method (LECO TC-436AR).

Electron diffraction (ED) and HRTEM observation were carried out on a field-emission Hitachi-1500 instrument operated at 800 kV. HRTEM image simulation was performed using the MacTempas simulation package based on the multi-slice calculation method. The simulated images presented herein were chosen near the Scherzer defocus of − 590 nm for the crystal thickness that resulted in the best match to the experimental observation.

3. RESULTS AND DISCUSSION

3.1. Powder Synthesis

Single phase of the new compound could be obtained in a wide range of boron content if the boron/carbon ratio is controlled between 6:1 to 16:1. In some cases, a small amount of ReB_4, ReB_6, or ReB_{12} coexisted with the new phase in the final product as mentioned before. A small amount of B_4C, which cannot be removed, was found in the cases with high carbon content. Chemical analysis of the best sample with smooth background and sharp peaks of the XRD pattern revealed a composition of $Y_{0.86}B_{22}C_{2.24}N_{0.59}$. The final structure analysis results show that the stoichiometric ideal composition of the new phase is $YB_{22}C_2N$, and the N atoms can also be replaced with C. The reaction temperature was controlled at around 1700°C. If the temperature was raised to higher than 2000°C, YB_4, YB_6, and B_4C appeared in the final product. This may be due to the decomposition of the new phase and such a fact may suggest that a single crystal of the new phase is difficult to prepare using the conventional melt growth method.

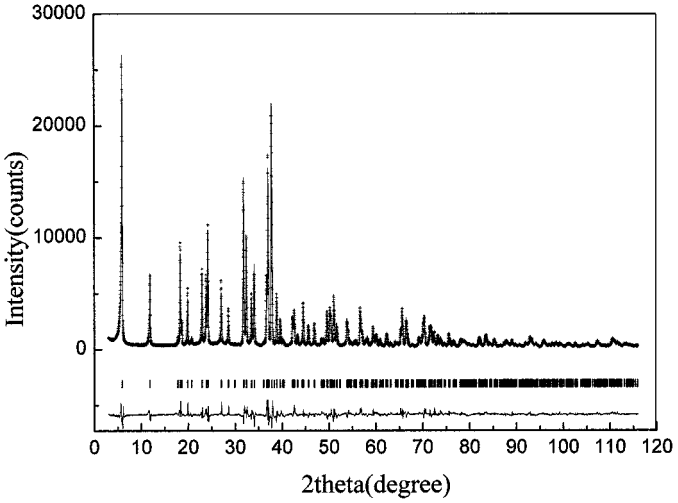

FIG. 1. Observed, calculated, and difference of the XRD profiles for the 12R phase of $YB_{22}C_2N$: (+) symbols represent the observed pattern; (—) is the calculated pattern; vertical bars show the Brag positions. The lowest solid line corresponds to difference spectra.

3.2. Structure Model and Analysis

The observed XRD pattern of the new phase with composition of $Y_{0.86}B_{22}C_{2.24}N_{0.59}$ is shown in Fig. 1 as (+) symbols. The starting Bragg peak at around 5.9° suggested a relatively large unit cell for the phase. All the diffraction peaks could be well indexed, using program TREOR90 (14), with a monoclinic structure of $a = 15.45$, $b = 8.91$, $c = 5.79$ Å and $\beta = 104.48°$. However, if the maximum length of unit cell parameter is set at 50 Å, the new phase could be well indexed with another high symmetry system, trigonal with $a = b = 5.6232$, $c = 44.7765$ Å, and the figure of merits (15, 16) for the indexing are M20 = 37, F20 = 54. The indexing results, which contain the observed, calculated d values of the peaks and their relative intensities are listed in Table 1. Further structure analysis also indicated that the latter unit cell choice is more suitable for expressing the crystal structure of the new phase. The extinction rule in the new phase shows that it belongs to rhombohedral symmetry with five possible space groups: $R3$, $R\text{-}3$, $R32$, $R3m$, and $R\text{-}3m$. A reasonable model could be built on the highest symmetry space group of $R\text{-}3m$ (No. 166), which is the same as that of α-boron (17) and other boron-rich borides such as B_4C (3, 18) and B_6O (2).

The mass density of the powders was measured by the conventional buoyance method using deionized water as a medium. The results lie between approximately 2.60 and

TABLE 1
Results of Indexing $YB_{22}C_2N$ with a Trigonal Unit Cell ($a = b = 5.6232$ Å, $c = 44.7765$ Å), and I Corresponds to Experimental Intensities

h	k	l	d_{obs}	d_{cal}	I/I_0	h	k	l	d_{obs}	d_{cal}	I/I_0
0	0	3	14.9172	14.9218	98	2	1	4	1.8158	1.8163	18
0	0	6	7.4644	7.4615	27	1	0	23	1.8078	1.8074	12
0	0	9	4.9733	4.9742	5	1	1	19		1.8061	
1	0	1	4.8335	4.8413	40	2	0	17	1.7879	1.7878	25
1	0	2	4.7604	4.7586	11	2	1	6		1.7870	
0	0	10		4.4775		2	1	7	1.7685	1.7689	10
1	0	4	4.4624	4.4655	24	2	1	10	1.7025	1.7024	12
1	0	7	3.8703	3.8744	31	2	0	19	1.6932	1.6933	6
0	0	12	3.7293	3.7306	29	1	0	26		1.6236	
1	0	8	3.6717	3.6737	50	2	1	13		1.6233	
1	0	10	3.2948	3.2958	28	3	0	0	1.6232	1.6233	19
1	0	11	3.1207	3.1229	17	3	0	1		1.6222	
1	0	13		2.8120		3	0	3	1.6138	1.6138	7
1	1	0	2.8117	2.8117	69	1	1	24	1.5547	1.5544	11
1	1	1		2.8060		3	0	9	1.5424	1.5432	5
1	1	3	2.7626	2.7630	46	2	1	16	1.5373	1.5378	6
1	0	14	2.6728	2.6729	24	2	0	23	1.5204	1.5204	5
0	0	17		2.6338		1	0	28		1.5193	
1	1	6	2.6301	2.6311	31	3	0	12	1.4887	1.4885	6
1	1	9	2.4467	2.4477	32	1	1	27	1.4285	1.4282	10
1	0	16	2.4263	2.4261	86	2	1	20	1.4216	1.4217	19
1	1	10		2.3810		2	0	26	1.4060	1.4059	13
2	0	4	2.3792	2.3794	100	2	2	0		1.4058	
1	0	17		2.3167		2	2	1		1.4051	
2	0	6	2.3156	2.3148	24	2	2	3		1.3996	
1	1	11		2.3134		0	0	33	1.3568	1.3566	5
2	0	7	2.2751	2.2756	13	2	2	10	1.3413	1.3413	11
2	0	10	2.1387	2.1391	14	3	1	4		1.3409	
1	0	19	2.1215	2.1210	17	3	0	19		1.3368	
2	0	11	2.0897	2.0896	6	3	0	20	1.3140	1.3141	7
0	0	22		2.0352		2	0	29	1.3039	1.3038	8
1	0	20	2.0343	2.0338	21	3	1	9		1.3034	
2	0	13	1.9877	1.9882	11	3	0	21	1.2916	1.2915	6
2	0	14	1.9372	1.9372	12	2	1	25	1.2835	1.2835	5
1	0	22	1.8776	1.8776	5	2	1	26		1.2574	
2	0	16	1.8364	1.8368	16	3	1	13	1.2573	1.2574	7

2.85 g/cm^3, which suggests six formula units of $YB_{22}C_2N$ in one unit cell for the new phase.

In fact, it is difficult to solve any crystal structure accurately for the sample with so many light atoms of B, C, and N just from the powder XRD pattern. However, with the structural knowledge of a recently found phase in the same system, whose structure was solved from single-crystal XRD data of $ScB_{17}CN$ (13), it is possible for us to build a reasonable model just from high quality powder XRD data. In order to do that, EXPO (19, 20)—a combination software of EXTRA package and SIRPOW97 package—was used. The intensities of 211 diffraction peaks, in which 112 peaks are independent, were extracted from the profile in the 2θ range from 3° to 116° after the whole pattern was automatically divided into four intervals. The fitting results gave

TABLE 2
Refined Atomic Parameters of $YB_{22}C_2N$ from Powder XRD Profiles by Rietveld Method

Atom	Site	x/a	y/b	z/c	Occupation	B (Å^{-2})
Y	6*c*	0	0	0.349(2)	0.74(4)	0.62(5)
N	6*c*	0	0	0.401(3)	0.84(0)	0.95(8)
C1	6*c*	$\frac{2}{3}$	$\frac{1}{3}$	0.485(8)	1.16(4)	3.19(0)
B1	18*h*	0.223(6)	−0.223(6)	0.442(3)	1.0	2.37(0)
B2	18*h*	0.557(2)	0.442(8)	0.349(4)	1.0	2.37(0)
B3	18*h*	0.151(8)	0.303(6)	0.404(3)	1.0	2.37(0)
C2	6*c*	$\frac{2}{3}$	$\frac{1}{3}$	0.423(2)	0.99(6)	3.19(0)
B4	18*h*	0.438(0)	0.562(0)	0.379(0)	1.0	2.37(0)
B5	6*c*	$\frac{2}{3}$	$\frac{1}{3}$	0.454(2)	1.01(4)	2.50(4)
B6	18*h*	0.499(6)	0.500(4)	0.417(5)	1.0	2.37(0)
B7	18*h*	0.102(1)	−0.102(1)	0.468(5)	1.0	3.37(0)
B8	18*h*	0.334(9)	0.167(4)	0.494(7)	1.0	2.37(0)

Note. Space group: *R*-3*m*, $z = 6$, $a = b = 5.623(0)$ Å, $c = 44.785(3)$ Å, $R_B = 9.1\%$, $R_F = 11.5\%$, $R_p = 8.75$, and $R_{wp} = 11.4\%$.

$R = 9.82\%$, and Wilson statistics of the whole peaks results in the total thermal factor of B = 0.329 Å^{-2}. After one cycle of refinement using the default settings, the program gave complete 12 atom positions: 1 yttrium, 1 nitrogen, 2 carbon, and 8 boron atoms. The combined figure of merit (CFOM) could reach 0.97. Table 2 lists the 12 atomic positions in the asymmetric unit cell. A complete structure model built by the 12 atoms in space group of *R*-3*m* is shown in Fig. 2. Atoms of B1, B3, B4, and B6 form an icosahedral cluster, B7 and B8 atoms form another icosahedron, and atoms of B5 form an octahedral cluster. There are a total 12 layers of atomic clusters in one unit cell, including 9 layers of icosahedron separated by the 3 layers of octahedron into 3 intervals (the new structure is thus named as 12R). The centers of the icosahedral and octahedral clusters of the 12 layers in the unit cell are ($\frac{2}{3}$, $\frac{1}{3}$, 0.0763), ($\frac{1}{3}$, $\frac{2}{3}$, 0.1667), (0, 0, 0.2571), ($\frac{2}{3}$, $\frac{1}{3}$, $\frac{1}{3}$), ($\frac{1}{3}$, $\frac{2}{3}$, 0.4096), (0, 0, 0.5), ($\frac{2}{3}$, $\frac{1}{3}$, 0.5904), ($\frac{1}{3}$, $\frac{2}{3}$, $\frac{2}{3}$), (0, 0, 0.7430), ($\frac{2}{3}$, $\frac{1}{3}$, 0.8333), ($\frac{1}{3}$, $\frac{2}{3}$, 0.9238), and (0, 0, 1.0), respectively. All boron atoms in the up and bottom triangles of icosahedron are bonded with boron atoms in the same sites of icosahedron in neighboring layers through bonds B1–B7. Unlike *Re*B_4 and *Re*B_6, all the atoms in the octahedron in the 12R phase are linked with icosahedra through the conventional bond B2–B4. The interconnected boron icosahedra and octahedra compose the three-dimensional framework of the crystal. Metal atoms reside in the voids of the boron framework, which lie in the octahedron layers. Similar to the structure of B_4C, 6 icosahedra in two neighboring layers are linked with C1–B5–C2 chains through bonds of C1–B8 and C2–B6, and the B6 and B8 atoms lie in the equatorial site of icosahedron. Each nitrogen atom is bonded with three boron atoms in the euqatorial site of three neighboring icosahedra, and each is also bonded with metal atoms. Such a structure model is

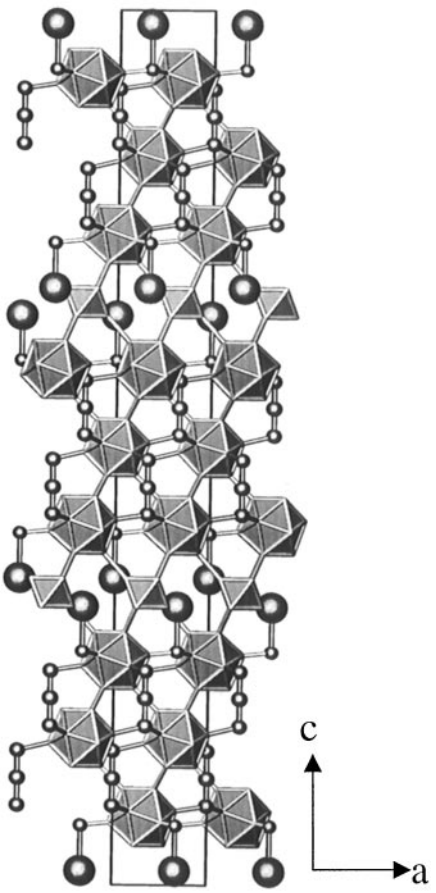

FIG. 2. Schematic diagram of crystal structure of 12R phase: (—) represents unit cell; the big and small polyhedra show boron icosahedra and octahedral, respectively; the three bonded atoms along the long [110] axis are C–B–C chains; the big atoms represent *Re* and the smaller atoms bonded with them are nitrogen.

very similar to that of newly found $ReB_{17}CN$ (13). In that case, each two icosahedral layers are separated by one boron octahedral layer and there are a total of 3 layers of boron clusters in one unit cell and the space group is *P*-3*m*1. This gave us confidence in the present structure model based on crystal chemical considerations.

The above structure model derived from direct method was refined with program FULLPROF (21). After background reduction, 41 parameters, including unit cell parameters, overall scale factor, peak shape, asymmetry, thermal factors, atomic sites, and occupation rates were refined. In fact, it is impossible to refine the thermal factors of all the light atoms individually; we set one value for all the boron atoms in the icosahedron and octahedron and the same for the two carbon atoms in the C–B–C chain. The intraicosahedral and intraoctahedral sites are considered fully occupied. The observed and calculated patterns and their differences are shown in Fig. 1. The final fitting results gave values of $R_p = 8.75\%$, $R_{wp} = 11.4\%$, $R_B = 9.1\%$, and $R_F = 11.5\%$. The detailed information of XRD data collection and structural refinement are listed in Table 3. The calculated composition according to the refined occupancies is in reasonable agreement with that of chemical determined.

The selected bond lengths are listed in Table 4. The icosahedral cluster I, formed by atoms of B1, B3, B4, and B6, are slightly distorted with B–B bonding lengths of $\sim$1.766(2) to $\sim$1.911(2) Å (average value: 1.828(4) Å) and bonding angles from $\sim 56.98^\circ$ to $\sim 64.46^\circ$. The average bonding distance in icosahedron II, which was built by atoms of B7 and B8, is 1.755(7) Å and the bonding angle is $56.5^\circ \sim 62.4^\circ$. The bond lengths of intraoctahedron are 1.788(8) and 1.846(5) Å. The bond lengths of intericosahedra and between icosahedra and octahedral are 1.664(9) and 1.762 Å, respectively. They are slightly shorter than intraicosahedra and intraoctahedra bond lengths, which is a typical bonding characteristic of "two electrons, three centers" bond of boron. The average C–B distance in the C–B–C chain is only 1.402 Å, much shorter than that of normal value. This phenomenon was also found in other boron–carbon systems (18, 22). The short C–B separation in the chains is not due to possible double-bond behavior. The theoretical model of B_4C (23) pointed out that the chain-center boron appeared to be a "positive" charged and the B^+ ion squeezed into a region between one or two relatively more electronegative carbon atoms with a loosely held central atom. This view of "soft" and weak binding of the boron chain center is supported by the early inelastic neutron scattering study of B_4C single crystals (24).

The boron octahedra in the new phase of 12R are different from those in ReB_4 and ReB_6 and each of them is strongly bonded with six icosahedra in neighboring layers. The new structure is very stable even in boiled nitric acid,

TABLE 3
Crystal Data and Structural Refinement for the 12R Phase of $YB_{22}C_2N$

Identification code	12R
Empirical formula	$YB_{22}C_2N$
Formula weight	364.77
Temperature	293 K
Wave length	1.54056 Å/1.54433 Å (Cu Kα/Kβ)
2θ range, number of points	$3 \sim 116$, 5651
Step width, sampling time	0.02, 6 s
Total and independent Brag peaks	211/112
Crystal system, space group	Hexagonal, *R*-3*m* (No. 166)
Unit cell dimensions	$a = 5.6230$ Å, $c = 44.7853$ Å
Volume	1226.19 Å^3
Z, Calculated density	6, 2.97 Mg/m^3
Programs	Treor90, EXPO97, Fullprof
Refinement method	Least square
Peak shape function	Pseudo-Voigt
Number of refined parameters	41
R values	$R_p = 0.0875$, $R_{wp} = 0.114$, $R_B = 0.091$, $R_F = 0.115$

TABLE 4
Selected Interatomic Distances in 12R Phase of $YB_{22}C_2N$

Atom–Atom	Distance (Å)	Atom–Atom	Distance (Å)
Icosahedron I		Chain	
B1–B1	1.8516	C1–B5	1.4152
B1–B3	1.8390	C2–B5	1.3888
B1–B6	1.8085		
B3–B4	1.9112	*Others*	
B3–B6	1.7976	Y–Y	3.5450
B4–B4	1.7662	Y–N	2.3118
B4–B6	1.8250	Y–B2	2.7369
		Y–B3	2.8766
Icosahedron II		Y–B4	2.9388
B7–B7	1.7225	N–B3	1.4864
B7–B8	1.8449	C1–B8	1.6636
B8–B8	1.6996	B2–B4	1.7623
		B1–B7	1.6649
Octahedron		C2–B6	1.6476
B2–B2	1.8177		

while the boron octahedra in ReB_4, ReB_6, and boron cubooctahedra in ReB_{12} are not so stable and can be dissolved in hot nitric acid. Powder synthesis results revealed that other rare earth elements such as Ho, Er, Tm, and Lu can also form the new 12R structure. While Yb cannot form the same structure, this may be due to the large ionic radius of Yb. Figure 3 shows the XRD patterns of the 12R phase together with that of $YB_{22}C_2N$. The unit cell parameters are listed in Table 5. However, although this is different from the $ReB_{17}CN$ phase (13), we have not found the 12R phase in Sc system. This may because that there are too many other phases in the boron-rich Sc–B–C system (8, 9, 13), and some structures are very stable in a wide composition range, which may suppress the formation of the 12R phase in this system.

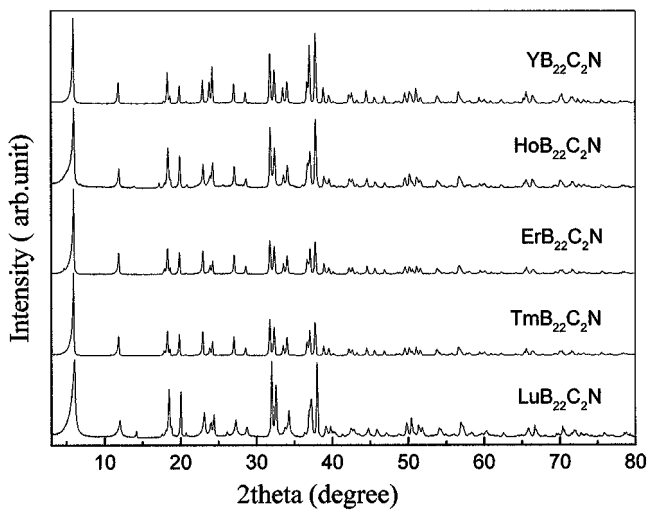

FIG. 3. Powder XRD patterns of $ReB_{22}C_2N$ (*Re*: Y, Ho, Er, Tm, and Lu). The similarities between them reveal that all of them are isostructural with $YB_{22}C_2N$.

TABLE 5
Unit Cell Parameters of $ReB_{22}C_2N$ (*Re*: Y, Ho, Er, Tm, Lu) Derived from Powder XRD

Re	*a* (Å)	*c* (Å)	*c*/*a*	*V* (Å^3)
Y	5.623(0)	44.785(3)	7.965	1226.19
Ho	5.614(9)	44.625(5)	7.948	1248.40
Er	5.626(4)	44.681(9)	7.942	1224.96
Tm	5.631(5)	44.737(9)	7.945	1228.72
Lu	5.595(7)	44.464(6)	7.946	1205.74

3.3. TEM Analysis

TEM analysis results also verified the rhombohedral unit cell. The most interesting structure character of the 12R phase is the layered stacking of boron clusters along the long *c* axis. Figure 4b shows the HRTEM image and the corresponding electron diffraction pattern along the [110] direction. In the ED pattern, every fourth diffraction spot along the *c* axis is stronger than the other three spots corresponding to 12R crystal periodicity, even though the ED pattern remained a strong monoclinic character. The 12R character can be seen more clearly in the HRTEM image, where one dark layer and three light layers are periodically stacking. The black spots in the dark layer represent Y atoms and the boron octahedral and the three fainter spots surrounded with bright zig-zags can be assigned as the three boron icosahedral layers and the C–B–C chains between them. The [001] direction of 12R phase is quite difficult to be found by TEM because of the long *c* axis. Figure 4a shows the HRTEM image along the [001] direction together with the corresponding ED pattern. In the HRTEM image, the black dots generated by Y atoms show a hexagonal symmetry which is in agreement with our structural model. The 12R phase is a semiconductor and the details of HRTEM image along this direction is not very clear. The inserted simulated pictures based on the above structure model matches the observed HRTEM image very well.

3.4. The Cooperation of Nitrogen Atom

The powder synthesis results showed that the formula of the new structure can be written as $Y_{1-x}B_{22}C_{3-y}N_{1-z}(0 \le x \le 0.7,\ 0 \le y \le 1,\ 0 \le z \le 1)$. The great change of B/Y ratio is due to the partial occupation of the Y sites. Just like B_4C (18, 23–25), the B/C ratio in the new structure can also change within a wide range. This may be

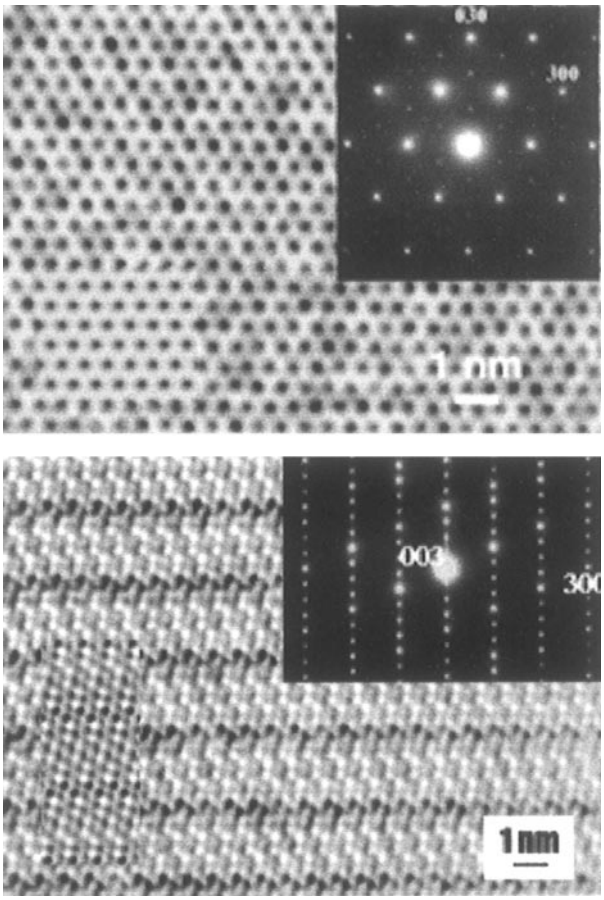

FIG. 4. Selected area electron diffraction pattern, image of HRTEM, and its simulation of the 12R phase along the (a) [001] and (b) [110] direction.

caused by the substitution between B and C in the new structure; that is, B_{12} icosahedron can be replaced with $B_{11}C$ and the C–B–C chain can be replaced with the C–B–B chain.

In the newly found quaternary system of $ReB_{17}CN$, the nitrogen atoms are essential for the phase formation. In order to know how important the nitrogen cooperation is in the new phase of $ReB_{22}C_2N$, we only used Y–B–C as the starting materials and we used a graphite crucible instead of the BN crucible. A single 12R phase can also be obtained as the final product. There is not enough nitrogen coming from the environment to create any nitrided phase because the crucible and the susceptor are all made of graphite and the reaction is performed in a vacuum of 10^{-4} Pa. Chemical analysis results show, under such a condition, the nitrogen in the final product is less than 0.1 wt%. Therefore, nitrogen atoms are not essential for the formation of the new 12R phase. Structure resolution results also indicate that nitrogen can be replaced with carbon and the nominal composition then corresponds to $ReB_{22}C_3$.

3.5. Magnetic Property Measurement

In the 12R phase, rare earth atoms form two-dimensional layers which are separated by about 15 Å, and they are expected to be magnetically almost independent of each other. In contrast, within the layer, the interatomic distance between each atoms is only 3.5 Å. Some magnetic anomalies caused from two-dimensional magnetic interaction may be expected. In fact, recently, an antiferromagnetic-like transition at a relatively high temperature of 17 K was found in boron-rich solids of TbB_{50} (26), where rare earth atoms are also rather sparse. In order to check if there is any unusual magnetic properties for 12R phase, the magnetic susceptibility of $TmB_{22}C_2N$ was measured using a superconducting quantum interference device (SQUID) magnetometer from 300 to 1.8 K under a magnetic field of 50 G. The static magnetic susceptibility vs temperature curve of $TmB_{22}C_2N$ is shown in Fig. 5. The magnetic susceptibility increases as the temperature decreases and a large change such as that observed in TbB_{50} at low temperature was not found in the sample. In fact, it should be mentioned also that no magnetic anomaly was found down to 1.8 K in $ErB_{17}CN$ (13) whose crystal structure is similar to the above-mentioned 12R phase. In order to determine the effective magnetic moment, the higher temperature values can be well fitted as the sum of a temperature-independent term χ_0 and Curie–Weiss term

$$\chi = \chi_0 + N\mu_{eff}/3K_B(T - \theta),$$

with $\chi_0 = 7.8 \times 10^{-3}$ emu/Tm mole, an effective number of Bohr magnetons μ_{eff} of $7.44\mu_B$/Tm atom, and a Curie–Weiss temperature θ of -6.5 K The magnitude of μ_{eff} shows good agreement with the value of $7.56\mu_B$/Tm

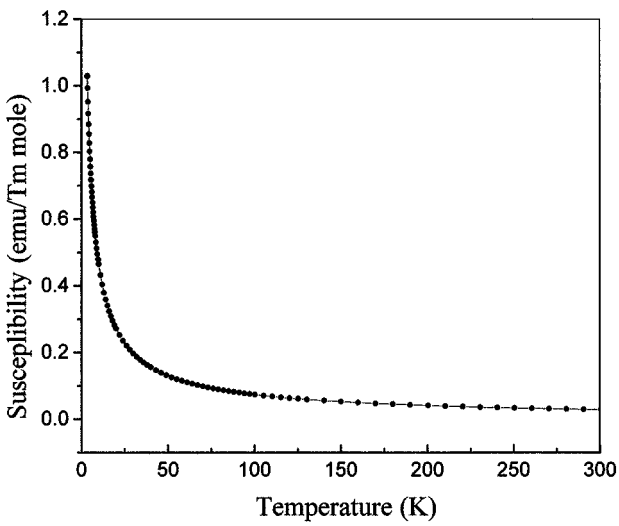

FIG. 5. Temperature dependence of the static magnetic susceptibility of $TmB_{22}C_2N$.

atom of free Tm^{3+} and indicates that the thulium atoms in the 12R phase are trivalent ions.

4. CONCLUSION

A new family of boron-rich solids with the formula $ReB_{22}C_2N$ or $ReB_{22}C_3$ was found by solid-state reaction. The crystal structure of $YB_{22}C_2N$ was solved from XRD data and confirmed by TEM observations. It shows a layered structure with rhombohedral symmetry. The boron atoms form nine layers of icosahedral and three layers of octahedral clusters in the framework. The interconnected icosahedral layers are linked with C–B–C chains. The nitrogen atoms which connect icosahedra and bonding with rare earth metallic atoms can be replaced with carbon.

ACKNOWLEDGMENTS

The first author acknowledges the support of STA fellowship by JST. We also thank Dr. M. Onoda for useful discussions, Dr. T. Sato for the preparation of the BCN precursor as the starting material, and Mr. S. Takenouchi for chemical analysis. We also appreciate the useful discussion with Dr. Petro Salamakha for the Rietveld refinement.

REFERENCES

1. P. Rogl, "Phase Diagram of Ternary Metal–Boron–Carbon Systems." ASM International, Materials Park, OH, 1998.
2. H. Hubert, B. Devouard, L. A. Garvie, M. O'Keeffe, P. R. Buseck, W. T. Petuskey, and P. F. McMillan, *Nature* **391,** 376 (1998).
3. R. J. Nelmes, J. S. Loveday, R. M. Wilson, W. G. Mashall, J. M. Besson, S. Klotz, G. Hamel, T. L. Aselage, and S. Hull, *Phys. Rev. Lett*. **74**(12), 2268 (1995).
4. C. Mailhiot, J. B. Grant, and A. K. McMahan, *Phy. Rev. B* **42,** 9033 (1990).
5. P. F. McMillan, H. Hubert, A. Chizmeshya, W. T. Petuskey, L. A. Garvie, and B. Devouard, *J. Solid State Chem.* **147,** 281 (1999).
6. D. Emin, *Phys. Today*, 55 (1987).
7. T. Tanaka, *J. Alloys and Compds.* **270,** 132 (1998).
8. Y. Shi, A. Leithe-Jasper, and T. Tanaka, *J. Solid State Chem.* **148,** 250 (1999).
9. A. Leithe-Jasper, L. Bourgeois, Y. Michiue, Y. Shi, and T. Tanaka, *J. Solid State Chem.* **154,** 130 (2000).
10. E. Bidaud, K. Hiebl, R. D. Hoffmann, R. Pottgen, C. Jardin, J. Bauer, R. Gautier, P. Gougeon, J. Y. Saillard, and J. F. Halet, *J. Solid State Chem.* **154,** 286 (2000).
11. J. Bauer, G. Boucekkine, G. Frapper, J. F. Halet, J. Y. Saillard, and B. Zouchoune, *J. Solid State Chem.* **133,** 190 (1997).
12. P. Rogl and F. Bouree, *J. Alloys and Compds.* **298,** 160 (2000).
13. A. Leithe-Jasper, T. Tanaka, L. Bourgeois, T. Mori, and Y. Michiue, *J. Solid State Chem*., in press (2000).
14. P.-E. Werner, L. Eriksson, and M. Westdahl, *J. Appl. Crystallogr.* **18,** 367 (1985).
15. P. M. de Wolf, *J. Appl. Crystallogr.* **1,** 108 (1968).
16. G. S. Smith and R. L. Snyder, *J. Appl. Crystallogr.* **12,** 60 (1979).
17. D. E. Sands and J. L. Hoard, *J. Amer. Chem. Soc.* **79,** 5582 (1957).
18. G. H. Kwei and B. Morosin, *J. Phys. Chem.* **100,** 803 (1996).
19. A. Altomare, M. C. Burla, G. Cascarano, C. Giacovazzo, A. Guagliardi, A. G. G. Moliterni, and G. Polidori, *J. Appl. Crystallogr.* **28,** 842 (1995).
20. A. Altomare, G. Cascarano, C. Giacovazzo, A. Guagliardi, M. C. Burla, G. Polidori, and M. Camalli, *J. Appl. Crystallogr.* **27,** 435 (1994).
21. J. Rodrguez-Carvajal, "FULLPROF," Version 3.2, 1997.
22. Y. Shi, L. Bourgeois, A. Leithe-Jasper, Y. Bando, and T. Tanaka, *J. Alloys and Compds.* **298,** 99 (2000).
23. D. Emin, *Phys. Rev. B* **38**(9), 6041 (1998).
24. C. W. Jr. Tucker and P. Senio, *Acta Crystallogr.* **8,** 371 (1955).
25. D. R. Tallant, T. L. Aselage, A. N. Campbell, and D. Emin, *Phys. Rev. B* **40**(8), 5649 (1989).
26. T. Mori and T. Tanaka, *J. Alloys and Compds.* **288,** 32 (1999).